



## Restoring Force Model for Seismic Performance of Corroded Steel Frame Columns



Pengfei Wang<sup>ID</sup>, Xiaofei Wang<sup>\*</sup><sup>ID</sup>, Wei Chen<sup>ID</sup>, Jing Shi<sup>ID</sup>

Department of Civil Engineering & Architecture, Nanyang Normal University, 473061 Nanyang, China

\* Correspondence: Xiaofei Wang (wangxiaofei870102@163.com)

Received: 07-25-2024

Revised: 09-08-2024

Accepted: 09-23-2024

**Citation:** P. F. Wang, X. F. Wang, W. Chen, and J. Shi, "Restoring force model for seismic performance of corroded steel frame columns," *GeoStruct. Innov.*, vol. 2, no. 3, pp. 144–160, 2024. <https://doi.org/10.56578/gsi020304>.



© 2024 by the author(s). Published by Acadlore Publishing Services Limited, Hong Kong. This article is available for free download and can be reused and cited, provided that the original published version is credited, under the CC BY 4.0 license.

**Abstract:** Corrosion-induced damage significantly impairs the seismic performance of steel frame columns, leading to an increased vulnerability during earthquake events. To address this issue, a restoring force model was developed to accurately describe the seismic behaviour of corroded steel columns. Low-cycle repeated loading tests were conducted on corroded steel frame columns to evaluate the effects of corrosion and earthquake-induced damage on their seismic performance. The results revealed distinct degradation patterns, which were systematically analyzed. A cyclic degradation index was proposed to quantify the impact of corrosion on critical parameters, including yield strength, hardening stiffness, unloading stiffness, and reloading stiffness. This index was incorporated into a damage model, which facilitated the formulation of a comprehensive restoring force model for corroded steel frame columns. The developed model was validated through case studies, demonstrating its effectiveness in predicting the seismic response of corroded columns. The findings underscore the importance of considering corrosion damage in the assessment and design of steel frame columns subjected to seismic loading, providing a more accurate and reliable approach for seismic performance evaluation.

**Keywords:** Corroded steel frame columns; Restoring force model; Seismic and corrosion coupling damage; Skeleton curve; Hysteresis rule

### 1 Introduction

Corrosion is one of the primary factors affecting the durability of steel structures. It degrades the mechanical properties of steel, reduces the cross-sectional area of components, and ultimately leads to a significant deterioration in the load-bearing capacity and seismic performance of steel structures [1–5]. Despite many anti-corrosion measures, the aging steel frames exposed in an aggressive corrosion environment still suffer serious corrosion, especially the exterior components [6]. Wang et al. [7] investigated the hysteretic behavior of corroded steel under cyclic loading and ultimately established a plastic constitutive model for corroded steel. The results showed that corrosion reduces the strength, ductility, and hysteretic energy of steel. Wang et al. [8] also studied the seismic performance of corroded steel columns. The results showed that corrosion causes the steel columns to enter various stages prematurely, worsening the buckling deformation range and reducing the load-carrying capacity and energy dissipation. Zhang et al. [9], Zheng et al. [10] and Zhang et al. [11] studied the seismic performance of corroded steel frame columns in marine atmospheric environments. The results showed that corrosion significantly reduces the bending capacity and ductility of the columns, leading to a more severe degradation of strength and stiffness. Xu et al. [12] conducted low-cycle fatigue loading tests to study the seismic performance of corroded steel columns. The results showed that as the degree of corrosion increases, the deformed area of the flange and web decreases, leading to a reduction in the ultimate bearing capacity and stiffness of the steel columns.

A restoring force model refers to a model that simplifies the key properties of the restoring force curve obtained from experiments using mathematical methods. This model is an essential tool for performing elastic-plastic analysis and dynamic time-history analysis of structures or components [13]. Currently, the research on restoring force models for steel structures or components is well-established [14–18], but studies focusing on the restoring force characteristics of existing or corroded steel structures or components remain scarce. Several studies have examined the restoring force characteristics of corroded steel frame beams in acidic atmospheres and established a hysteresis skeleton curve model [15, 19]. Compared to beams, columns play a more crucial role in the seismic performance of

steel frame structures. Therefore, it is urgent to establish a restoring force model for steel frame columns that can reflect damage due to corrosion. Zheng et al. [20] investigated the seismic behavior of steel frame columns with varying degrees of corrosion through cyclic loading tests. It was found that the seismic resistance of corroded steel frame columns decreases as the degree of corrosion increases. Moreover, the hysteretic curves and those curves of skeleton, strength degradation, stiffness degradation, and hysteretic energy dissipation of corroded frame columns differ significantly from those of the non-corroded frame. To more accurately describe the seismic behavior of corroded steel frame columns, there is an urgent need for a restoring force model that specifically addresses these structures. This model would help in understanding how corrosion affects the seismic performance of steel columns, including changes in their strength, stiffness, and energy dissipation capabilities.

In light of this, based on the conclusions drawn from the low-cycle loading tests of steel frame columns with varying degrees of corrosion reported in the study by Zheng et al. [20], the effects of coupled seismic and corrosion damage on the seismic behavior of steel frame columns were considered. This study builds upon the damage index-based restoring force model proposed by Takeda et al. [21]. A method for determining the cyclic degradation index of corroded steel frame columns was developed based on the damage model of such columns. Subsequently, the bilinear restoring force model was refined, leading to the establishment of a restoring force model specifically for corroded steel frame columns. This advancement aims to provide a more precise tool for evaluating the seismic performance of corroded steel structures, taking into account the complex interactions between corrosion and seismic forces.

## 2 Experiment Overview of Corroded Steel Frame Columns

Zheng et al. [20] designed 12 steel frame columns, and the design variable of four steel frame columns is the degree of corrosion. The design parameters are shown in Table 1.

**Table 1.** Design parameters of steel frame columns

Specimen Number	Steel Specification	Steel Grade	Axial Compression Ratio	Corrosion Degree	Corrosion Time/h
Column-10	HW250×250×9×14	Q235B	0.2	Non-corrosion	0
Column-1	HW250×250×9 14	Q235B	0.2	Slight corrosion	320
Column-2	HW250×250×9	Q235B	0.2	Severe corrosion	960

### 2.1 Specimen Design

Steel frame columns with HW250×250×9×14 cross-section were designed in the test. In order to ensure the failure of the frame columns during the test, a bottom beam with larger rigidity was made at the bottom of the columns. Q235 steel was used for section steel specimens and steel plates. The section size of the specimens is shown in Figure 1.

### 2.2 Accelerated Corrosion Test Plan

In order to obtain the steel frame columns with different corrosion degrees, the columns need to be corroded. Due to the long period of the actual atmospheric exposure test, in order to shorten the test time and truly predict the steel corrosion to a certain extent, indoor accelerated corrosion method was used in the test. The acid atmospheric corrosion test of all specimens in this test was conducted in the ZHT / W 2300 climate simulation experiment system, as shown in Figure 2.

#### 2.2.1 Preparation of the test corrosion solution

##### (a) 5% neutral sodium chloride (NaCl) solution

NaCl was dissolved in distilled water or deionized water with a temperature of  $25^{\circ}\text{C} \pm 2^{\circ}\text{C}$  and a conductivity of no more than  $20 \mu\text{s}/\text{cm}$ , and prepared into a solution with a concentration of  $50 \text{ g/L} \pm 5 \text{ g/L}$ . At  $25^{\circ}\text{C}$ , the density range of NaCl solution was  $1.029\text{-}1.036 \text{ g/cm}^3$ .

NaCl solution shall not contain more than 0.001% (mass fraction) of copper and nickel. The content of copper and nickel shall be determined by atomic absorption spectrometry or other methods with the same sensitivity. In addition, NaCl shall not contain more than 0.1% (mass fraction) of sodium iodide or more than 0.5% (mass fraction) of total impurities calculated relative to dry salt.

If the PH value of the prepared solution at  $25^{\circ}\text{C} \pm 2^{\circ}\text{C}$  exceeds the range of 6.0~7.0, the content of impurities in the water shall be detected.

##### (b) Acidification

At  $25^{\circ}\text{C} \pm 2^{\circ}\text{C}$ , the PH value of the solution shall be adjusted to  $3.5 \pm 0.1$ , and the following reagents shall be added to 10 L 5% neutral NaCl solution: (i) 12 ml nitric acid solution ( $\text{HNO}_3, \rho = 1.42 \text{ g/cm}^3$ ); (ii) 17.3 ml sulfuric

acid solution ( $\text{H}_2\text{SO}_4$ ,  $\rho=1.84 \text{ g/cm}^3$ ); (iii) 10% sodium hydroxide solution ( $\rho=1.1 \text{ g/cm}^3$ ), and the PH value of the solution shall be adjusted to  $3.5 \pm 0.1$  (about 300 ml sodium hydroxide solution is required).

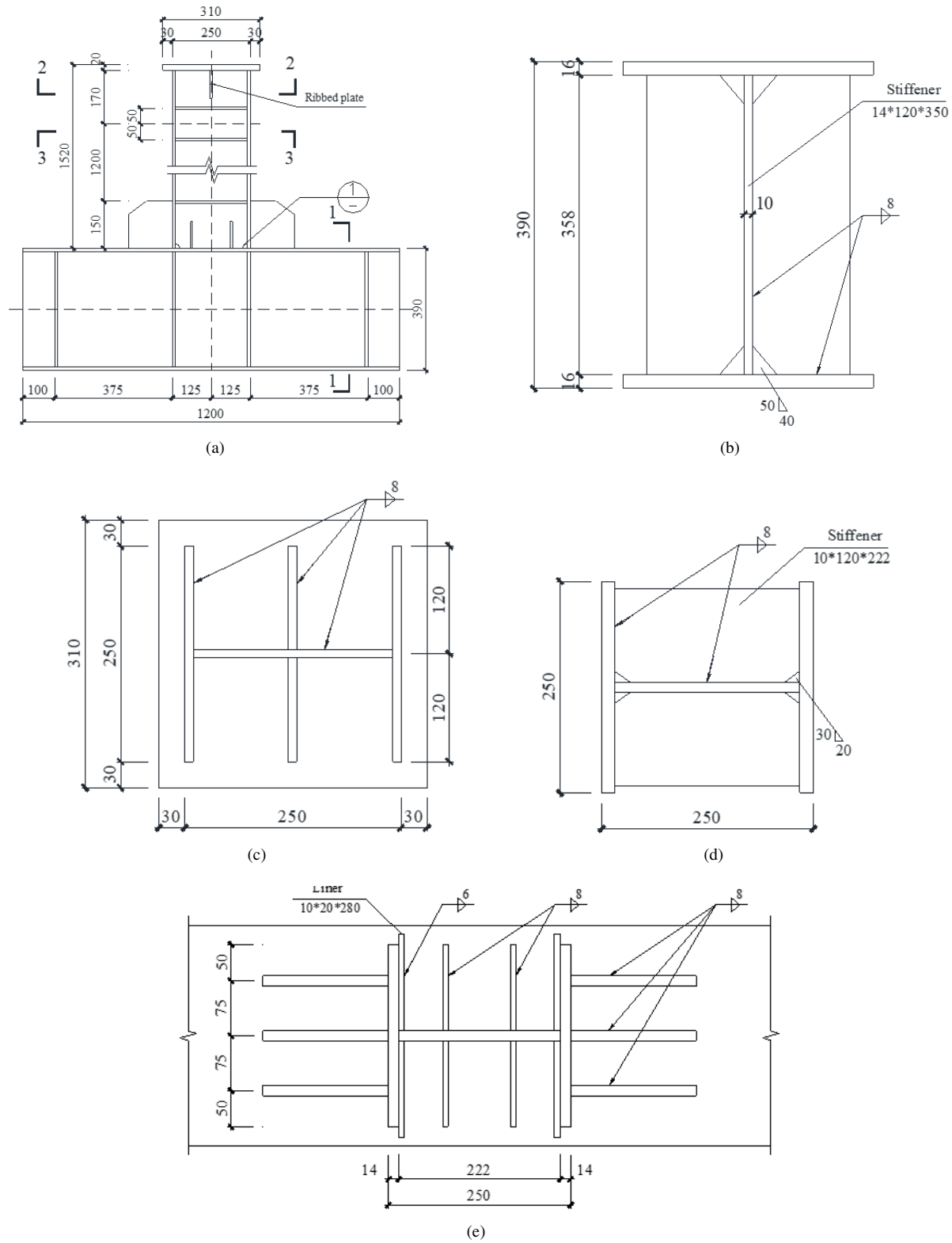


**Figure 1.** Sectional dimensions of specimens: (a) specimen elevation; (b) 1-1 profile; (c) 2-2 profile; (d) 3-3 profile; and (e) details of the column base

## 2.2.2 Continuity of test

(a) During the whole test period, it is better not to interrupt the test. If the test process needs to be interrupted for sampling inspection, the interruption time shall be as short as possible.

(b) If the end of the test depends on the time at which corrosion begins, the specimens should be inspected frequently.

(c) The samples with predetermined test cycle can be inspected by visual inspection regularly, but during the inspection, the sample surface cannot be damaged, and the time and times of unpacking inspection shall be minimized.

## 2.2.3 Settling velocity of salt spray

After spraying with 24 hours, the deposition rate of salt spray on each 80 cm<sup>2</sup> is 1~2 mL/h. Use of the spray solution should be ceased.

## 2.2.4 Test cycle

The corrosion test was repeated for 120 cycles, with 8 hours for each cycle and totally 960 hours. The duration was 2 hours for the acid salt spray, 4 hours for the dry condition, and 2 hours for the wet condition. The specific parameters are shown in Table 2.

The corrosion process is shown in Figure 3.



**Figure 2.** ZHT / W2300 climate simulation system



**Figure 3.** Specimen corrosion process

**Table 2.** Parameters of the periodic salt spray composite corrosion test

Content	Test Conditions
NaCl solution	5% (mass percentage)
PH value of solution	3.5 ~ 3.6
Acid salt spray state	Time: 2 h ; spray: 5 min; and interval: 5 min
Moist state	Time: 2 h ; temperature: 50°C ± 5°C, and humidity: >95% RH
Drying state	Time: 4 h; temperature: 60°C ± 5°C; and humidity: <30% RH Acid salt spray state→drying state: <30 min
Test state transition interval	Drying state→moist state: <15 min Moist state→ acid salt spray state: <30 min

### 2.3 Loading System

The loading diagram and device of the frame columns in the quasi-static test are shown in Figure 4 and Figure 5.

The variable amplitude displacement control loading system was adopted in this quasi-static test, and the specific loading process is shown in Figure 6.

### 2.4 Test Content and Test Instrument Layout Plan

The test contents of this quasi-static test included horizontal displacement and load of the steel frame column top, and strain of the column base flange and web, etc. Among them, the horizontal displacement and the load of the steel frame column top were output and collected by the displacement load sensor of MTS electro-hydraulic servo actuator. The arrangement of the measuring points and the strain gauges at the flange and the web of the column base is shown in Figure 7.

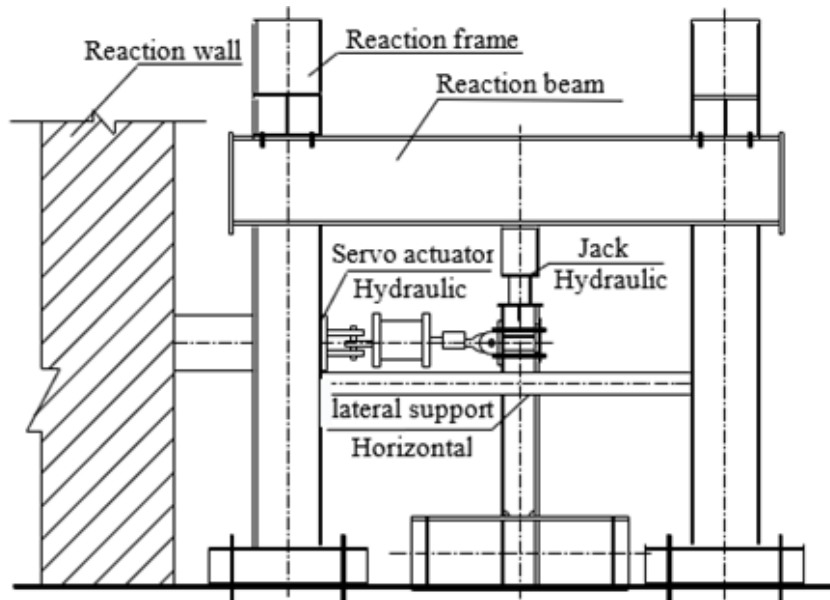
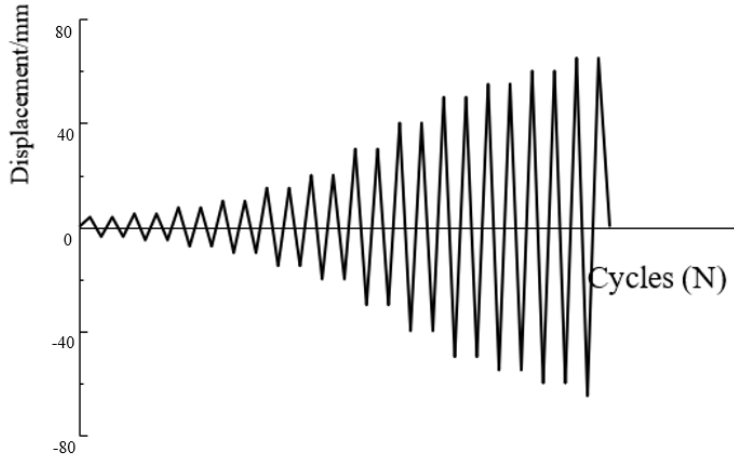


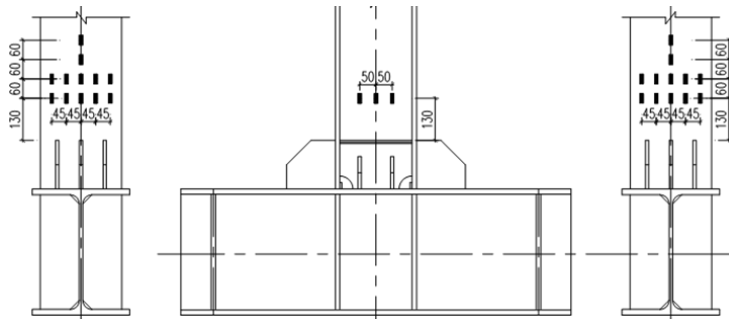
Figure 4. Diagram of the test loading device



Figure 5. Actual test loading device



**Figure 6.** The variable amplitude displacement control loading process



**Figure 7.** Arrangement diagram of the strain gauge of the columns base web and the flange

### 3 Damage Model of Corroded Steel Frame Columns

Zheng et al. [22] obtained an earthquake damage model for corroded steel structures by modifying the seismic damage model proposed by Ou et al.:

$$D_\eta = \left( \frac{x_{m,\eta}}{X_{u,\eta}} \right)^{\beta_1} + \left( \frac{E_{h,\eta}}{F_{y,\eta} X_{u,\eta}} \right)^{\beta_1} \quad (1)$$

where,  $D_\eta$  is the damage value of the steel frame column with a corrosion rate of  $\eta$ ;  $x_{m,\eta}$  and  $E_{h,\eta}$  are the maximum horizontal displacement and the maximum hysteretic energy dissipation of the steel frame column with a corrosion rate of  $\eta$  under earthquake action; and  $X_{u,\eta}$  and  $F_{y,\eta}$  are the ultimate horizontal displacement and the yield shear stress of the steel frame column with a corrosion rate of  $\eta$ . The definition and calculation formula of the corrosion rate  $\eta$  of H steel are detailed in the study by Zheng et al. [22].

### 4 Establishment of the Restoring Force Model Considering Damage

The damage restoring force model, which has gained recognition and widespread use, is a restoring force model based on a damage index proposed by Takeda et al. [21] in 1978, as illustrated in Figure 8. This model is characterized by the yield point not being constant but decreasing as the damage degree increases, pointing to the latest yield point under reverse loading. This feature allows the model to effectively describe the impact of seismic damage on the seismic performance of structures.

Using the characteristics of the above-mentioned damage restoring force model for reference, based on the experimental results [20] and the damage model of corroded steel frame structures [21], the bilinear restoring force model was improved from two aspects of skeleton curve and hysteretic rule. Finally, the restoring force model of corroded steel frame columns considering damage was established.

#### 4.1 Determination of Skeleton Curve

By comparing the skeleton curves of steel frame columns with different corrosion degrees, as shown in Figure 9 [20], it can be observed that while the skeleton curves of corroded and non-corroded components are

similar, the extent of performance degradation under cyclic loading differs, leading to variations in the model parameter values. The differences in the skeleton curve model parameters between corroded and non-corroded components are reflected below. Compared to non-corroded components, the strength and stiffness of corroded components degrade more rapidly under seismic loads. The deformation capacity and the energy dissipation ability of corroded components are reduced. As the degree of corrosion increases, these phenomena become progressively more pronounced. Ultimately, the failure mode of the component shifts from ductile to brittle failure.

Based on the test skeleton curves, the skeleton curve of corroded steel frame columns was simplified into a bilinear skeleton curve model with a hardening section, as depicted in Figure 10.

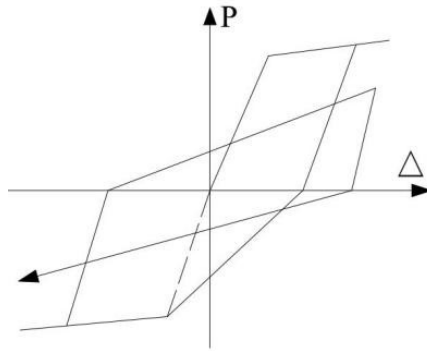


**Figure 8.** Damage restoring force model

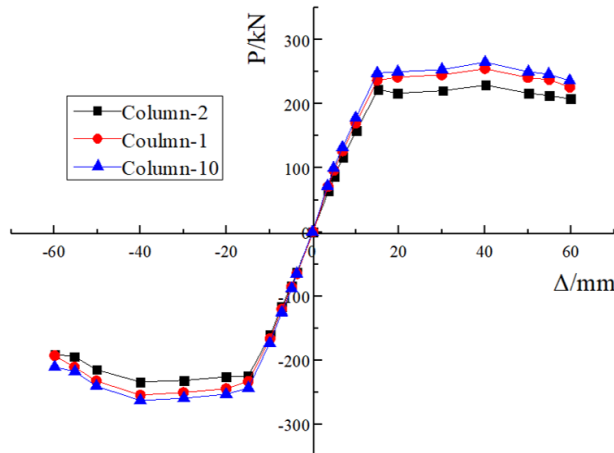


**Figure 9.** Comparison of skeleton curves of specimens with different corrosion degrees

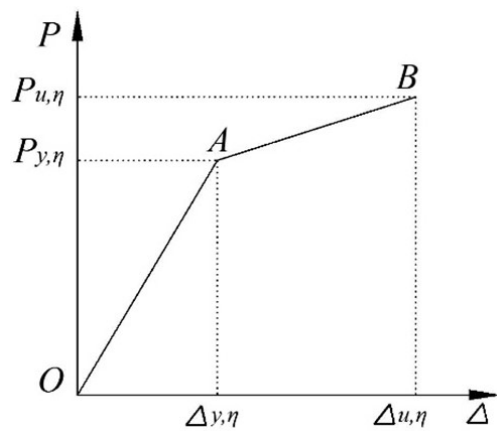


**Figure 10.** Simplified skeleton curve and characteristic points of corroded steel frame columns

The bilinear skeleton curve model with hardening section can be divided as follows:

(a) Elastic stage

As can be seen from Figure 9, all specimens have no significant deformation before yielding, they are basically in the elastic stage, and the slope of the loading curve is basically constant. Therefore, the skeleton curve of the steel frame column before yielding can be simplified as the connection line from the coordinate origin to the yield point, that is, the OA straight line segment in Figure 10. The stiffness of this stage is the initial stiffness  $K_{y,\eta}$ :

$$K_{y,\eta} = P_{y,\eta}/\Delta_{y,\eta} \quad (2)$$

where,  $K_{y,\eta}$  is the initial stiffness of the frame column with a corrosion rate of  $\eta$ ;  $P_{y,\eta}$  is the yield load of the frame column with a corrosion rate of  $\eta$ ; and  $\Delta_{y,\eta}$  is the yield displacement of the frame column with a corrosion rate of  $\eta$ .

(b) Hardening stage

When the specimen is yielding, the specimen appears plastic deformation compared with the initial stiffness, and the stiffness of the specimen is smaller at this time. This stage can be simplified as the connection between the yield point  $(P_{y,\eta}, \Delta_{y,\eta})$  and the peak load point  $(P_{u,\eta}, \Delta_{u,\eta})$ , that is, the AB segment in Figure 10. The stiffness of this stage is the hardening stiffness, which is used to describe the tensile toughening effect of the structural member after yielding. The following expression can be obtained between the hardening stiffness and the initial stiffness:

$$K_{u,\eta} = \alpha_{s,\eta} K_{y,\eta} \quad (3)$$

where,  $K_{u,\eta}$  is the hardening stiffness of the frame column with a corrosion rate of  $\eta$ ; and  $\alpha_{s,\eta}$  is the hardening coefficient of the frame column with a corrosion rate of  $\eta$ . In this study, it is assumed that  $\alpha_{s,\eta}=\alpha_s$ , and  $\alpha_s$  is the hardening coefficient of the non-corroded steel column, with  $\alpha_s=0.025$ .

The calculation method for the characteristic points in Formulas (2) and (3) and the skeleton curve in Figure 10 is detailed in the study by Takeda et al. [21].

## 4.2 Simplification of the Hysteretic Curve

Figure 11 shows the hysteretic curves of steel frame columns with different degrees of corrosion. As can be seen from Figure 11, the hysteretic loops of all steel frame columns are basically close to the spindle shape. The hysteretic curves under cyclic horizontal loading are essentially symmetrical and can be basically divided into two parts: the yielding stage and the limit stage. Compared with non-corroded steel frame columns, the hysteretic loops of the corroded ones are flatter, and the energy dissipation capacity is lower. Before yielding, the loading and unloading curves of the specimens are almost close to the straight line, and the slope of the straight line is almost constant. The slopes of the loading and unloading curves are the initial stiffness and the unloading stiffness, with the initial stiffness being basically the same as the unloading stiffness. When the specimens are yielding, the loading and unloading curves of the hysteresis loops have the following characteristics:

a) Loading curve: When the specimen is yielding, the slope of the loading curve (i.e., the load stiffness) decreases with the increase of the cycle number and the increase of the displacement amplitude, and the magnitude of the decrease increases gradually. Comparison of the hysteretic curves of specimens with different corrosion degrees shows that the curve slope decreases with the increase of corrosion degree under the same loading cycle times, which indicates that the attenuation rate of the specimen's stiffness increases with the increase of corrosion degree.

b) Unloading curve: When the specimen is yielding, the slope of unloading curve (i.e., unloading stiffness of specimen) decreases with the increase of the cycle number and the increase of the displacement amplitude. After complete unloading, there is a residual deformation in the specimen. In the unloading curve of the same direction, the residual deformation after the latter unloading is larger than the residual deformation after the previous unloading. Compared to the non-corroded steel column, the residual deformation of corroded steel frame columns is larger.

According to the characteristics of the hysteretic curves of corroded steel frame columns (Figure 11), the hysteretic curve is simplified, as shown in Figure 12.

As can be seen from Figure 12, the steel column has undergone three processes throughout the loading and unloading cycle, namely, elastic (0-1, 3-4, 6-7, 9-10), strengthening (1-2, 5-4, 7-8, 10-11), and unloading (2-3, 5-6, 8-9, 11-12). The corresponding stiffness of the above three stages is the initial stiffness (or loading stiffness), hardening stiffness and unloading stiffness.

As can be seen from the hysteretic curve in Figure 11, with the increase of loading cycle times and the increase of horizontal displacement amplitude, the loading stiffness, hardening stiffness, unloading stiffness, yield load and peak load of the specimens are continuously reduced. Therefore, in order to obtain the complete hysteretic curve of corroded steel frame columns, the degradation of the specimens' properties should be determined.

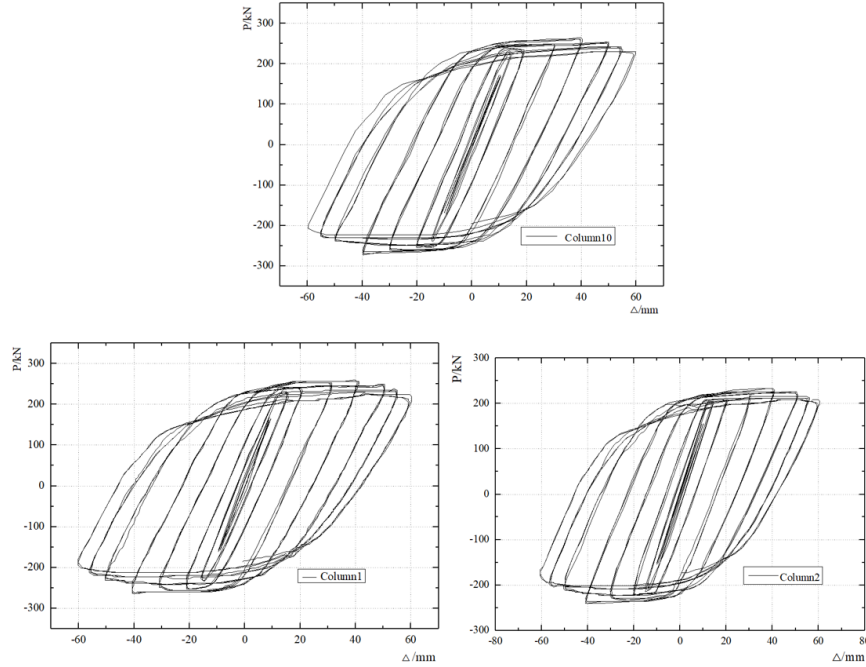


**Figure 11.** Hysteretic curves of steel frame columns with different corrosion degrees

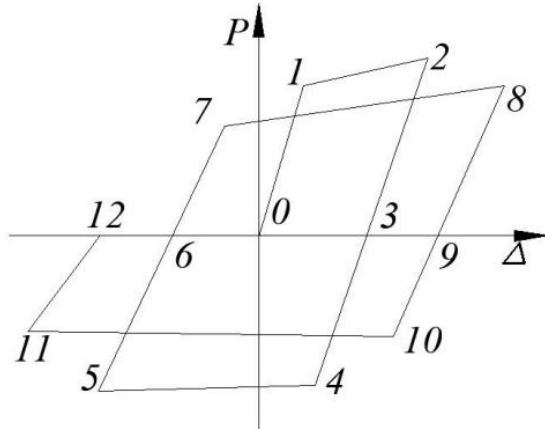


**Figure 12.** Simplified hysteretic loops of corroded steel frame columns

#### 4.3 Cyclic Degradation Index

In this study, the cyclic degradation index is used to quantitatively describe the degradation of corroded steel frame columns.

In establishing the restoring force model of steel reinforced high-strength concrete frame columns, the following cyclic degradation index was put forward based on the damage of specimen [13]:

$$\beta_i = [\Delta D_i / (1 - D_{i-1})]^\varphi \quad (4)$$

where,  $\Delta D_i$  is the increment of the damage value of the specimen at the  $i$ -th loading cycle;  $D_{i-1}$  is the cumulative damage value of the specimen before the  $i$ -th loading cycle; and  $\varphi$  is the correlation coefficient.  $\varphi=1.2$  was analyzed according to the test results. The cyclic degradation index is used to describe the performance degradation of specimen by using the damage degree of specimen under cyclic loading. At the same time, the influence of loading path on the cyclic degradation index was considered.

The above cyclic degradation index formula was reformed, and the cyclic degradation index of corroded steel frame columns was obtained:

$$\beta_{i,\eta} = [\Delta D_{i,\eta} / (1 - D_{i-1,\eta})]^\varphi \quad (5)$$

where,  $\Delta D_{i,\eta}$  is the increment of the damage value of the frame column with a corrosion rate of  $\eta$  at the  $i$ -th loading cycle, and its calculation method is shown in Formula (1);  $D_{i-1,\eta}$  is the cumulative damage value of the frame column with a corrosion rate of  $\eta$  before the  $i$ -th loading cycle; and  $\varphi$  is the correlation coefficient.  $\varphi=1.2$  was analyzed according to the test results [21].

The value of the cyclic degradation index  $\beta_{i,\eta}$  was between [0,1], and the value was closer to 1, which indicates that the performance degradation of the frame column is more serious. If  $\beta_{i,\eta} < 0$  or  $\beta_{i,\eta} > 1$ , it means that the damage value increment of frame column under a certain cyclic loading exceeds the residual damage value, and the frame column is invalid. Therefore, the failure criterion can be expressed as:

$$\Delta D_{i,\eta} > 1 - D_{i-1,\eta} \quad (6)$$

(a) Degradation of the yield load

By observing the hysteretic curves of corroded steel frame columns, it can be seen that the yield load decreases with the increase of loading cyclic number. The degradation law of the yield load is defined as:

$$P_{y(i,\eta)}^{\pm} = (1 - \beta_{i,\eta}) P_{y(i-1),\eta}^{\pm} \quad (7)$$

where,  $P_{y(i,\eta)}^{\pm}$  is the yielding load of the frame column with a corrosion rate of  $\eta$  at the  $i$ -th loading cycle;  $P_{y(i-1),\eta}^{\pm}$  is the yielding load of the frame column with a corrosion rate of  $\eta$  at the  $(i-1)$ -th loading cycle; and superscript “ $\pm$ ” represents the direction of loading, with “+” indicating positive loading and “-” indicating reverse loading.

(b) Degradation of the hardening stiffness

Like the yield load, the hardening stiffness of the specimens also decreases with the increase of loading cyclic number, and the degradation law of the hardening stiffness is defined as:

$$K_{u(i,\eta)}^{\pm} = (1 - \beta_{i,\eta}) K_{u(i-1),\eta}^{\pm} \quad (8)$$

where,  $K_{u(i,\eta)}^{\pm}$  is the hardening stiffness of the frame column with a corrosion rate of  $\eta$  at the  $i$ -th loading cycle; and  $K_{u(i-1),\eta}^{\pm}$  is the hardening stiffness of the frame column with a corrosion rate of  $\eta$  at the  $(i-1)$ -th loading cycle.

(c) Degradation of the unloading stiffness

The experimental results show that the unloading stiffness of corroded steel frame columns has no obvious degradation at the elastic stage, and the value is basically the same as the initial stiffness  $K_{y,\eta}$ . However, when the horizontal load reaches the yield load and the structure is in an elastic-plastic state, the unloading stiffness of the frame column decreases with the increase of loading cyclic number, and its degradation law can be described by the following formula:

$$K_{d(i,\eta)}^{\pm} = (1 - \beta_{i,\eta}) K_{d(i-1),\eta}^{\pm} \quad (9)$$

where,  $K_{d(i,\eta)}^{\pm}$  is the unloading stiffness of the frame column with a corrosion rate of  $\eta$  at the  $i$ -th loading cycle; and  $K_{d(i-1),\eta}^{\pm}$  is the unloading stiffness of the frame column with a corrosion rate of  $\eta$  at the  $(i-1)$ -th loading cycle.

(d) Degradation of reloading stiffness

From the hysteresis curve of Figure 11, it can be seen that the slope of forward unloading is consistent with that of the reverse reloading stiffness in any complete hysteresis loop in the whole loading cycle. The forward loading stiffness of the  $i$ -th cycle is approximately the same as the slope of the reverse unloading stiffness of the  $(i-1)$ -th cycle. Therefore, the degradation law of the reloading stiffness is expressed by the following formulas:

$$K_{ri,\eta}^- = K_{di,\eta}^+ \quad (10)$$

$$K_{ri,\eta}^+ = K_{d(i-1),\eta}^- \quad (11)$$

where,  $K_{ri,\eta}^{\pm}$  is the reloading stiffness of the frame column with a corrosion rate of  $\eta$  at the  $i$ -th loading cycle.

#### 4.4 Hysteresis Rule

Through the description of the degradation law of corroded steel frame columns, the restoring force model of corroded steel frame columns based on damage was obtained, as shown in Figure 12.

The hysteretic rule of corroded steel frame columns is as follows:

(a) The loading and unloading of corroded steel frame columns are carried out along the elastic section of the skeleton curve (i.e., 0-1 stage in Figure 12) before yielding.

(b) The first loading cycle of corroded steel frame columns after yielding is presented below. The loading stiffness of the 0-1 stage is taken as the loading stiffness at the elastic stage during forward loading, and the corresponding load value at point 1 and the hardening stiffness of the 1-2 stage, respectively, take the corresponding yield load and hardening stiffness of the specimen when it is first yielding. When unloading, the unloading stiffness of the 2-3 stage is the same as the loading stiffness of the 0-1 stage. In reverse loading, according to Formula (10), the reverse loading stiffness of the 3-4 stage is the same as the unloading stiffness of the 2-3 stage, and the yield load value of point 4 is the same as the loading value of point 1. However, the direction is opposite. The hardening stiffness of the 4-5 section is the same as that of the 1-2 section. In the reverse unloading stage, the unloading stiffness of the 5-6 stage is equal to the unloading stiffness of the 2-3 stage.

(c) The second loading cycle after yielding is presented below. According to Formula (11), the loading stiffness of the 6-7 stage is the same as that of the 5-6 unloading stage in the previous cycle loading. The damage model proposed by Karina et al. [2] was used to calculate the damage value increment  $\Delta D_{i-1}$  of the previous loading cycle and the damage increment  $\Delta D_i$  of this loading cycle. The corresponding degradation index  $\beta_{i,\eta}$  was calculated by Formula (5). The yield load at points 7 and 10, the hardening stiffness of 7-8 and 10-11 stages, and the unloading stiffness of 8-9 and 11-12 stages were calculated by Formulas (7), (8) and (9), respectively.

The loading cycle of the 3rd, 4th, ..., n-th after yielding is the same as that of the second after yielding. When the maximum horizontal bearing capacity of the specimen drops to 0.85 times the ultimate bearing capacity, the loading is stopped.

### 5 Validation of the Restoring Force Model

The restoring force model of corroded steel frame columns was validated by using the ABAQUS software.

#### 5.1 Material Parameters

According to the actual experimental requirements, the Q235B steel grade was selected. A bilinear hardening model was used as the material constitutive model for the steel used in the structural model, as shown in Figure 13. The material parameters for the uncorroded steel are listed in Table 3, where the density is  $7850 \text{ kg/m}^3$ , the Poisson's ratio is 0.3, and the tensile strength is 460 MPa.

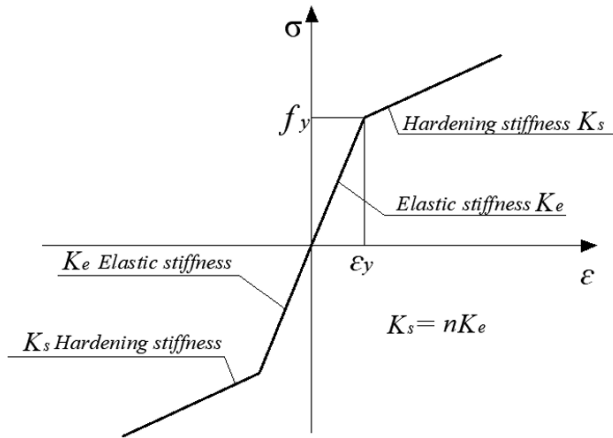


**Figure 13.** Bilinear hardening constitutive model

**Table 3.** Material properties of steel

	$K_e/\text{MPa}$	$f_y/\text{MPa}$	$n$
Column	$2.06 \times 10^5$	235	0.03

## 5.2 Element Meshing

In the process of establishing the specimen model, 3D solid elements with high precision was adopted in this study for elastic-plastic nonlinear analysis. Specifically, modified tetrahedral solid elements (C3D10M) were chosen, and the element shape is shown in Figure 14. This element type is suitable for contact and elastoplastic problems, offering high precision, although it comes with a higher computational cost. It is a commonly used element type for simulating the elastoplastic state of structural members. Ultimately, the element meshing of the test specimens is shown in Figure 15.

The same loading method was employed in this study for the finite element simulation of the test specimens used in the experimental section of the study by Takeda et al. [21].

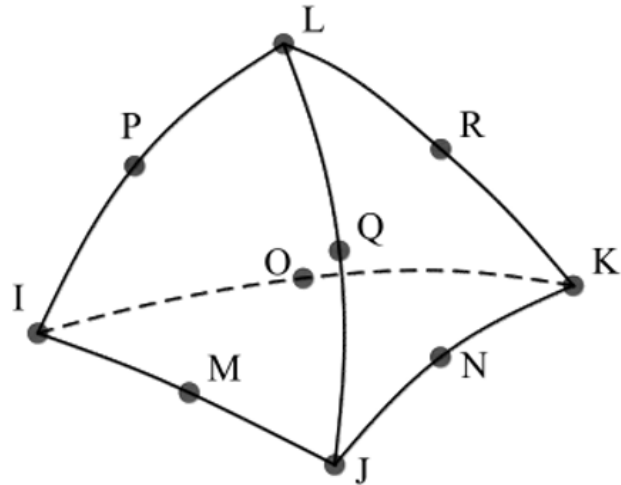


**Figure 14.** Schematic diagram of the C3D10M element model

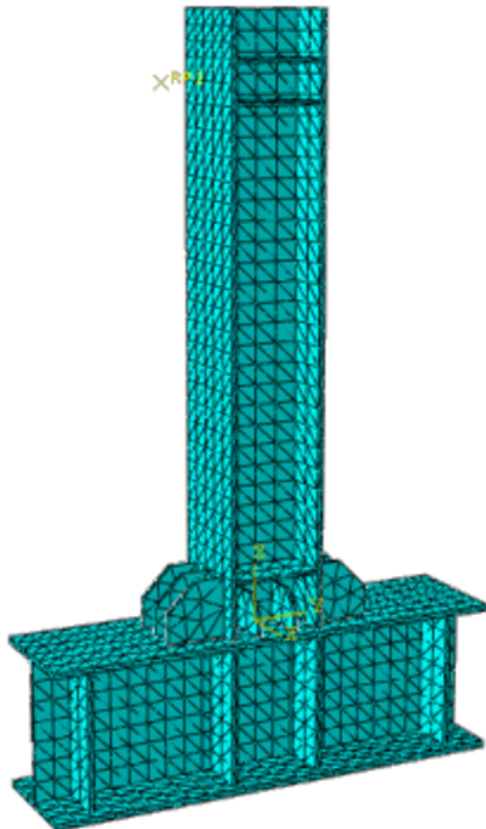


**Figure 15.** Meshing of the test specimen

### 5.3 Initial Defects of the Specimen

Steel materials may experience certain initial deformations during production and transportation, which can be referred to as initial defects of the steel. To perform more accurate finite element simulations of the test specimens and to accurately model the local yielding deformation of the columns, it is necessary to incorporate defect data into the model. The buckling modes of the model were calculated using the Buckle solver command in ABAQUS, as shown in Figure 16. Then, the \*IMPERFECTION keyword was used to add imperfection data to the model.

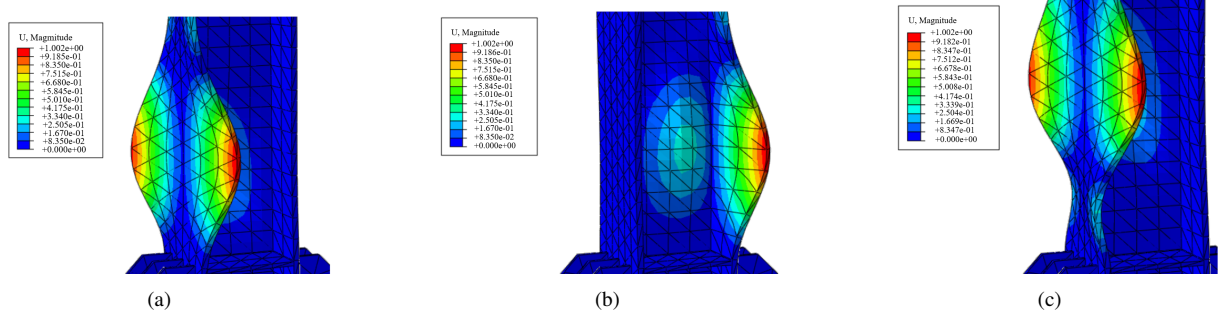


**Figure 16.** Buckling modes of the numerical model of the frame column: (a) first-order buckling mode; (b) second-order buckling mode; and (c) third-order buckling mode

### 5.4 Definition of the Restoring Force Model

In ABAQUS, a user subroutine (UMAT) written in Fortran was used to implement the mathematical expressions for the restoring force model of corroded steel frame columns. During the simulation, ABAQUS was used to call the user subroutine to compute the stress state at each time step.

### 5.5 Finite Element Analysis Results

#### 5.5.1 Failure modes

As shown in Figure 17, the comparison between the failure modes of the test specimens and those from the finite element simulations reveals that the morphologies are essentially consistent. By observing the failure photographs of the specimens and the finite element simulation images, it is evident that both exhibit similar failure patterns. This consistency further demonstrates the scientific validity and reliability of the finite element simulations.

#### 5.5.2 Hysteresis curve

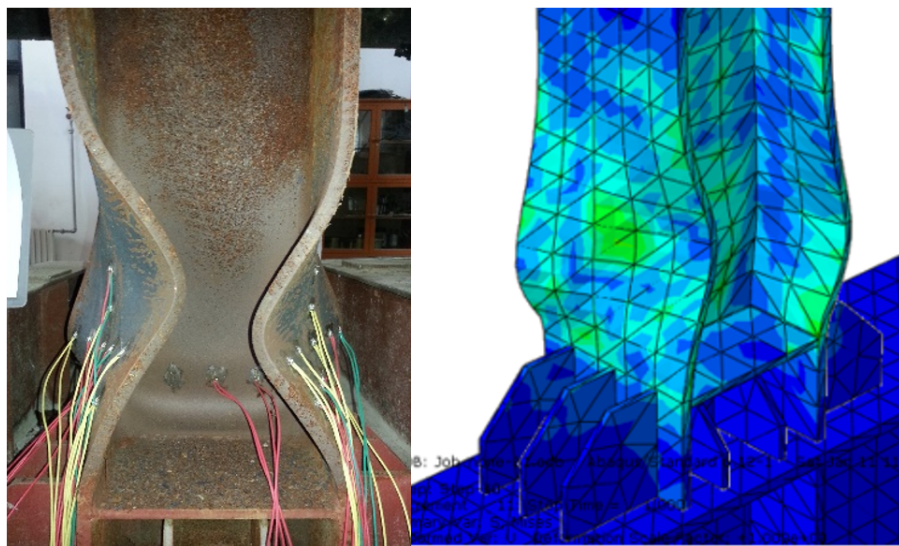
As shown in Figure 18, the hysteresis curves obtained from ABAQUS finite element simulations were compared with those from actual experimental tests for specimens with different design parameters.

As shown in Figure 18, the trends of the experimental curves and the finite element numerical simulation curves are largely consistent. Upon comparing the hysteresis curves from the finite element simulations, it is evident that the positive and negative hysteresis loops are symmetric about the origin, whereas the experimental curves exhibit discrepancies. In quasi-static tests, as the number of loading cycles increases, the specimens may gradually develop damage and deformation. These damages and deformations can affect the mechanical behavior of the specimens, leading to asymmetry in the hysteresis loops. For example, plastic deformation in the specimens can lead to different energy dissipation capacities during positive and negative loading. Additionally, friction and slip between the loading device and the specimens can affect the stress state and deformation patterns, further contributing to the asymmetry in the hysteresis loops. The hysteresis rules in the finite element simulations presented in this study consider only the effects of earthquake and corrosion damages on the seismic performance of the components, and do not account for potential asymmetry in the positive and negative loading cycles.

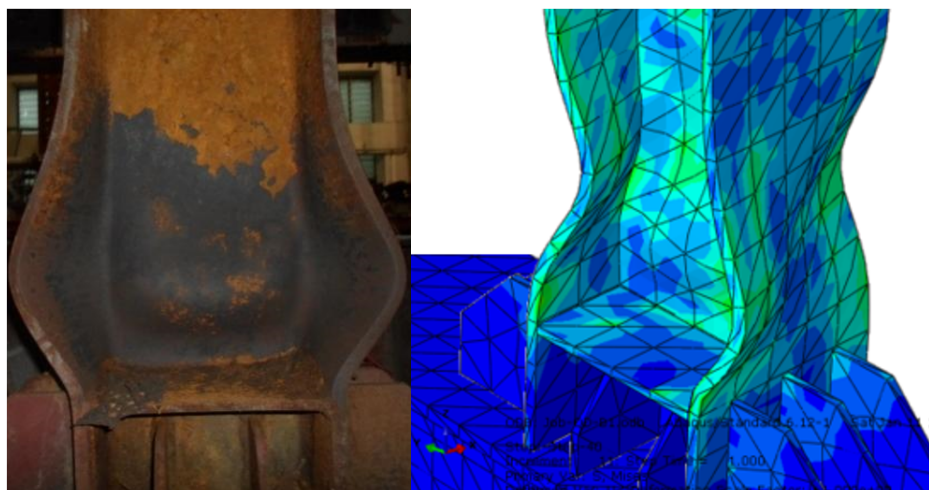
Table 4 provides the experimental and finite element computed values of characteristic points on the hysteresis curve. From the data in Table 4, it can be seen that the relative error between the computed and experimental values for all characteristic points is less than 6.19%, meeting the precision requirements.

From Figure 18, it can be seen that the computed hysteresis curves match the experimental results well, indicating that the restoring force model can effectively describe the hysteretic behavior of corroded steel frame columns under cyclic loading.

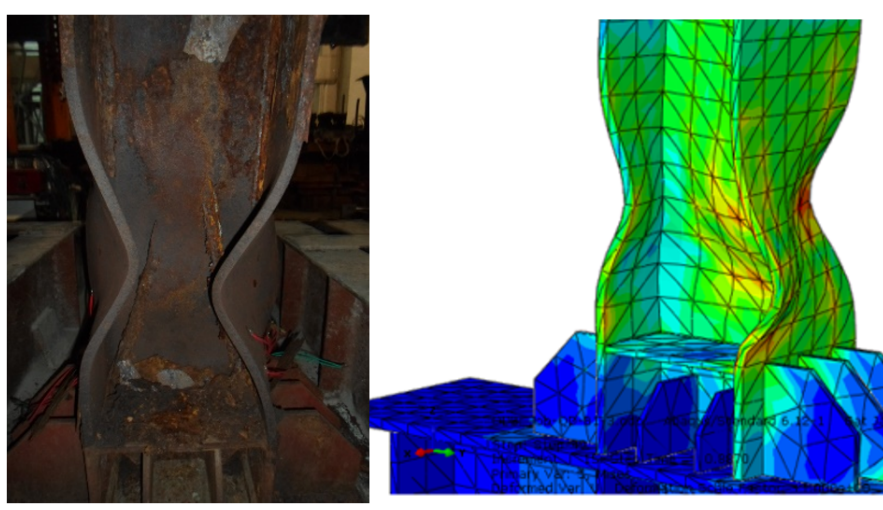
From Table 4, it can be observed that the values of the characteristic points on the skeleton curves, calculated using the restoring force model, decrease with increasing corrosion levels. This indicates that the restoring force model established in this study can effectively describe the influence of different corrosion levels on the seismic performance of steel frame columns.



(a)



(b)



(c)

**Figure 17.** Comparison of failure modes between experimental tests and finite element simulations: (a) column 10; (b) column 1; and (c) column 2

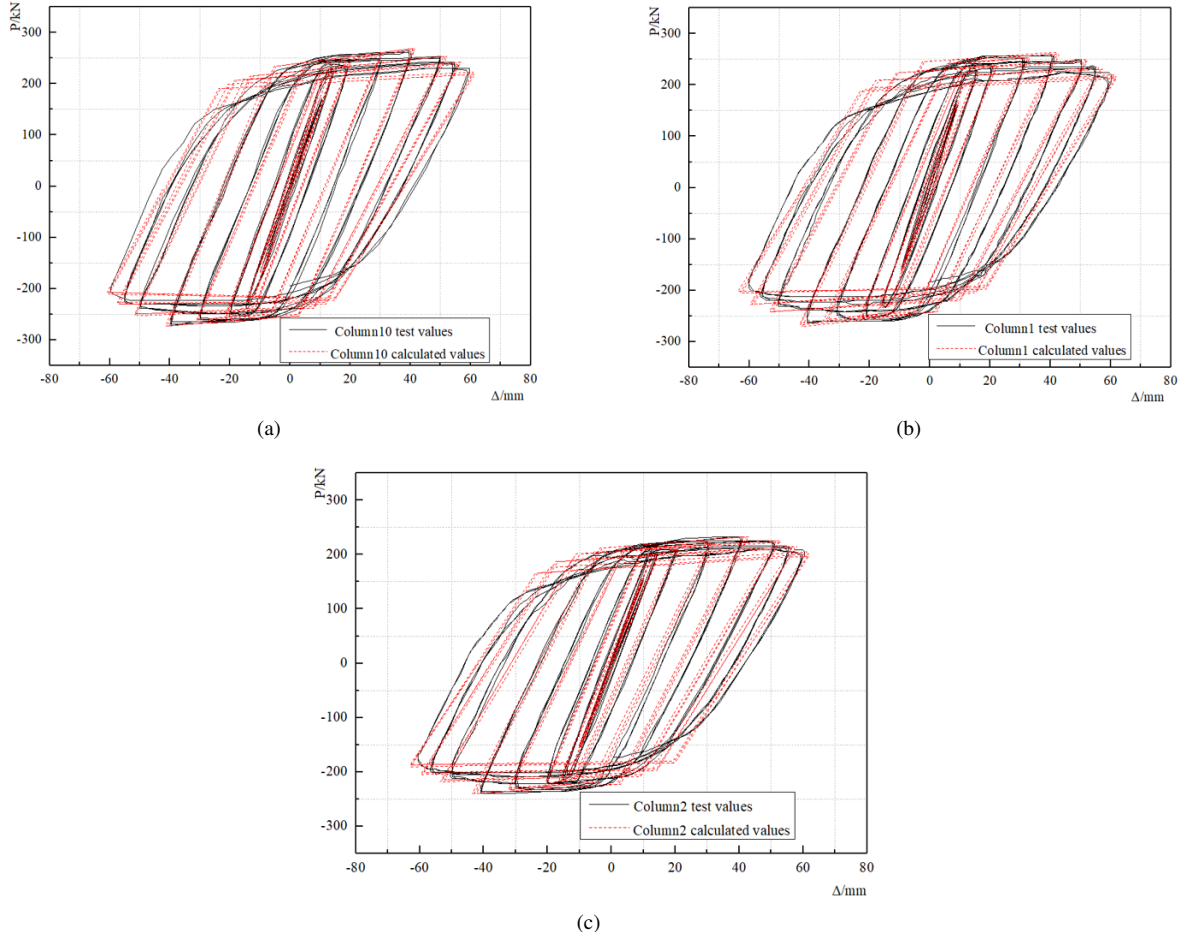


**Figure 18.** Comparison between calculated hysteresis curves and experimental hysteresis curves: (a) column 10; (b) column 1; and (c) column 2

**Table 4.** The ratio between the experimental and calculated values of the characteristic points of the skeleton curve

Value of Characteristic Points		F <sub>y</sub> /kN	Δ <sub>y</sub> /mm	F <sub>u</sub> /kN	Δ <sub>u</sub> /mm
Column 10	Test values	243.31	16.07	259.83	40.06
	Calculated values	241.05	15.96	257.13	39.55
	Relative error /%	-0.929%	-0.685%	-1.039%	-1.273%
Column 1	Test values	230.92	15.02	249.84	44.85
	Calculated values	227.49	15.58	246.71	43.54
	Relative error /%	-1.485%	3.738%	-1.253%	-2.921%
Column 2	Test values	218.93	14.06	226.61	40.10
	Calculated values	215.78	14.93	222.32	41.34
	Relative error /%	-1.439%	6.188%	-1.893%	3.092%

## 6 Conclusions

After analyzing and summarizing the skeleton curves of steel frame columns under different corrosion degrees, a restoring force model for corroded steel frame columns was established in this study. Compared to existing models, the innovation of the proposed restoring force model lies in that it is based on the damage model of corroded steel frames by establishing a cyclic degradation index formula. This formula describes the degradation patterns of yield strength, hardening stiffness, unloading stiffness, and reloading stiffness using the cyclic degradation index. The results from case studies demonstrate that the restoring force model developed in this study can effectively describe the seismic performance of corroded steel frame columns under earthquake loads.

By investigating the performance degradation patterns of corroded steel frame columns, this study revealed the significant impact of corrosion on the seismic performance of structures. These findings are crucial for engineers

involved in seismic design, as they highlight the importance of considering corrosion factors in their designs. Engineers can use these insights to implement necessary seismic measures, thereby enhancing the overall seismic capacity of structures.

The bilinear skeleton curve model and the cyclic degradation index formula developed in this study, which consider corrosion damage, are not only applicable to steel frame columns with specific corrosion degrees but also exhibit broad applicability. By adjusting the parameters in the model, it can be applied to steel frame columns with varying degrees of corrosion and different cross-sectional dimensions and material properties. This provides a powerful tool for evaluating the seismic performance of steel structures in corrosive environments. The research methodology presented in this study is not limited to steel frame columns but can be extended to other types of steel structural components, such as steel beams and joints. Using similar research methods, corrosion damage models can be established for various components, thereby further refining the evaluation system for the seismic performance of steel structures in corrosive environments.

The limitation of this study lies in the fact that the finite element simulation techniques did not adequately account for factors causing asymmetry in the positive and negative hysteresis loops of steel frame columns. Therefore, improvements to the finite element simulation techniques could consider additional influencing factors, such as non-uniform corrosion distribution and variability in material properties, to further investigate how to enhance the accuracy and reliability of the models.

## Author Contributions

Author Contributions: Conceptualization, P.W.; methodology, P.W. and X.W.; software, P.W. and W.C.; validation, X.W.; formal analysis, J.S.; investigation, W.C.; resources, P.W.; writing—original draft preparation, X.W.; writing—review and editing, P.W.; visualization, W.C. All authors have read and agreed to the published version of the manuscript.

## Funding

This research has been supported by Henan Provincial Science and Technology Research Project (Grant number: 242102321029; 242102230145; 242102241011), Key Scientific Research Project of Henan Higher Educational Institution (Grant No.: 24A580003), Special Project of Nanyang Normal University (Grant No.: 2022ZX024) and Research Teaching Demonstration Course of Nanyang Normal University (Grant No.: 2023-YJKC-010), which are gratefully acknowledged.

## Data Availability

The data used to support the research findings are available from the corresponding author upon request.

## Acknowledgements

I gratefully acknowledge the help of Yanzhao Han, who put forward valuable suggestions on the thesis.

## Conflicts of Interest

The authors declare no conflict of interest.

## References

- [1] L. Di Sarno, A. Majidian, and G. Karagiannakis, “The effect of atmospheric corrosion on steel structures: A state-of-the-art and case-study,” *Buildings*, vol. 11, no. 12, p. 571, 2021. <https://doi.org/10.3390/buildings11120571>
- [2] P. Chun, O. Kizuaki, and C. K. N. Nada, “Tensile strength prediction of corroded steel plates by using machine learning approach,” *Steel Compos. Struct.*, vol. 24, no. 5, pp. 635–641, 2017. <https://doi.org/10.3390/buildings11120571>
- [3] R. M. Pidaparti, , and A. S. Rao, “Analysis of pits induced stresses due to metal corrosion,” *Corros. Sci.*, vol. 50, no. 7, pp. 1932–1938, 2008. <https://doi.org/10.1016/j.corsci.2008.05.003>
- [4] R. Shahabi and K. Narmashiri, “Effects of deficiency location on CFRP strengthening of steel CHS short columns,” *Steel Compos. Struct.*, vol. 28, no. 3, pp. 267–278, 2018. <https://doi.org/10.12989/scs.2018.28.3.267>
- [5] S. Sultana, Y. Wang, A. J. Sobey, J. A. Wharton, and R. A. Shenoi, “Influence of corrosion on the ultimate compressive strength of steel plates and stiffened panels,” *Thin-Walled Struct.*, vol. 96, pp. 95–104, 2015. <https://doi.org/10.1016/j.tws.2015.08.006>
- [6] H. Karagah, C. Shi, M. Dawood, and A. Belarbi, “Experimental investigation of short steel columns with localized corrosion,” *Thin-Walled Struct.*, vol. 87, no. 11, pp. 191–199, 2015. <https://doi.org/10.1016/j.tws.2014.11.009>

- [7] Y. Wang, T. Shi, H. Zhang, B. Nie, H. Wang, and S. Xu, “Hysteretic behavior and cyclic constitutive model of corroded structural steel under general atmospheric environment,” *Constr. Build. Mater.*, vol. 270, p. 121474, 2021. <https://doi.org/10.1016/j.conbuildmat.2020.121474>
- [8] Y. Wang, T. Shi, B. Nie, H. Wang, and S. Xu, “Seismic performance of steel columns corroded in general atmosphere,” *Steel Compos. Struct.*, vol. 40, no. 2, pp. 217–241, 2021. <https://doi.org/10.12989/scs.2021.40.2.217>
- [9] X. Zhang, S. Zheng, X. Zhao, and Q. Yang, “Seismic performance and hysteretic model of corroded steel frame columns in offshore atmospheric environment,” *Adv. Struct. Eng.*, vol. 26, no. 16, pp. 3041–3064, 2023. <https://doi.org/10.1177/13694332231208249>
- [10] S. Zheng, X. Zhang, and X. Zhao, “Experimental investigation on seismic performance of corroded steel columns in offshore atmospheric environment,” *Struct. Des. Tall Spec. Build.*, vol. 28, no. 2, p. e1580, 2018. <https://doi.org/10.1002/tal.1580>
- [11] M. Zhang, S. Zheng, and X. Zhao, “Experimental and numerical investigations into seismic behavior of corroded steel frame beams and columns in offshore atmospheric environment,” *J. Constr. Steel Res.*, vol. 201, p. 107757, 2023. <https://doi.org/10.1016/j.jcsr.2022.107757>
- [12] S. Xu, Z. Zhang, and G. Qin, “Study on the seismic performance of corroded H-shaped steel columns,” *Eng. Struct.*, vol. 191, pp. 39–61, 2019. <https://doi.org/10.1016/j.engstruct.2019.04.037>
- [13] B. Wang, W. Huang, and S. Zheng, “Study on restoring force performance of corrosion damage steel frame beams under acid atmosphere,” *Appl. Sci.*, vol. 9, no. 1, p. 103, 2018. <https://doi.org/10.3390/app9010103>
- [14] Z. Yin, D. Feng, and Y. He, “Restoring force model of end-plate bolted shear links in eccentrically braced frames,” *J. Constr. Steel Res.*, vol. 199, p. 107623, 2022. <https://doi.org/10.1016/j.jcsr.2022.107623>
- [15] S. Jia, Y. Wang, X. Wang, and X. Liu, “Seismic behavior and restoring force model of connections between rectangular tubular columns and h-shaped beams using single direction bolts,” *J. Build. Struct.*, vol. 41, no. 5, pp. 168–179, 2020. <https://doi.org/10.14006/j.jzjgxb.2018.0365>
- [16] Y. Chen and C. Chen, “Restoring force model of prefabricated self-centering rocking steel moment-resisting frame,” *J. Build. Struct.*, vol. 42, no. 7, pp. 144–153, 2021. <https://doi.org/10.14006/j.jzjgxb.2019.0396>
- [17] Y. Shi, D. Su, and Y. Wang, “Study on restoring force models of steel beam-column connections with composite action,” *World Earthquake Eng.*, vol. 24, no. 2, pp. 15–20, 2008.
- [18] H. Li, Q. Ben, Z. Yu, Y. Zhang, and X. Lv, “Analysis and experiment of cumulated damage of steel frame structures under earthquake action,” *J. Build. Struct.*, vol. 25, no. 3, pp. 69–74, 2004.
- [19] S. Zheng, X. Liu, X. Zhang, J. He, and Y. Liu, “Study on restoring force model of Q235 steel frame beam in different corrosion degrees,” *J. Hunan Univ. (Nat. Sci.)*, vol. 46, no. 9, pp. 44–53, 2019. <https://doi.org/10.16339/j.cnki.hdxbzkb.2019.09.005>
- [20] S. Zheng, X. Wang, Y. Han *et al.*, “Experimental study on seismic behavior of multi-aged steel frame columns in acidic atmospheric environment,” *China Civ. Eng. J.*, vol. 48, no. 8, pp. 47–59, 2015. <https://doi.org/10.15951/j.tmgcb.2015.08.006>
- [21] T. Takeda, M. A. Sozen, and N. N. Nielson, “Reinforced concrete response to simulated earthquakes,” *J. Struct. Div., ASCE*, vol. 96, no. 12, pp. 2557–2572, 1970.
- [22] S. S. Zheng, X. F. Wang, Y. Cheng, and L. B. Sun, “Seismic damage model of a corroded steel frame,” *J. Vib. Shock*, vol. 34, no. 3, pp. 144–149, 2015. <https://doi.org/10.13465/j.cnki.jvs.2015.03.023>